APPLIED PHYSICS LETTERS 102, 043116 (2013)

Comparative study of chemically synthesized and exfoliated multilayer MoS_2 field-effect transistors

Wan Sik Hwang,[1,2,a)] Maja Remskar,[3] Rusen Yan,[2] Tom Kosel,[2] Jong Kyung Park,[4] Byung Jin Cho,[4] Wilfried Haensch,[1] Huili (Grace) Xing,[2] Alan Seabaugh,[2] and Debdeep Jena[2,b)]
[1]*IBM T. J. Watson Research Center, Yorktown Heights, New York 10598, USA*
[2]*Department of Electrical Engineering, University of Notre Dame, Notre Dame, Indiana 46556, USA*
[3]*Solid State Physics Department, Jozef Stefan Institute, Jamova 39, SI-1000 Ljubljana, Slovenia*
[4]*Department of Electrical Engineering, Korea Advanced Institute of Science and Technology, Daejeon 305-701, Korea*

(Received 26 November 2012; accepted 17 January 2013; published online 31 January 2013)

We report the realization of field-effect transistors (FETs) made with chemically synthesized multilayer 2D crystal semiconductor MoS_2. Electrical properties such as the FET mobility, subthreshold swing, on/off ratio, and contact resistance of chemically synthesized (s-) MoS_2 are indistinguishable from that of mechanically exfoliated (x-) MoS_2, however, flat-band voltages are different, possibly due to polar chemical residues originating in the transfer process. Electron diffraction studies and Raman spectroscopy show the structural similarity of s-MoS_2 to x-MoS_2. This initial report on the behavior and properties of s-MoS_2 illustrates the feasibility of electronic devices using synthetic layered 2D crystal semiconductors. © *2013 American Institute of Physics*. [http://dx.doi.org/10.1063/1.4789975]

Two-dimensional (2D) crystal materials are receiving increased attention for future electronic devices. Short-channel effects in modern transistors originate from the 3-dimensional (3D) nature of the gate control; introduction of 2D materials in the channel significantly improves the gate electrostatics. Graphene is a true 2D material,[1] but its lack of a bandgap results in high leakage in the off-state in conventional transistor geometries. Alternative switching mechanisms[2–4] could enable electronic switching with high on-off current ratios. 2D transition-metal dichalcogenide (TMD) materials such as MoS_2,[5,6] WSe_2,[7,8] and WS_2 (Refs. 9 and 10) have drawn considerable attention due to the presence of a bandgap, in contrast to graphene. Prior studies of TMD multilayered materials have been conducted using exfoliated layers,[5–9] similar to the initial work with graphene.[1] The size and quality of naturally occurring exfoliated layered semiconductor materials are limited and uncontrollable, so it is important to develop synthetic techniques. Multilayer TMDs, like graphite, are excellent solid lubricating materials and have been chemically synthesized in large volumes, but have not been investigated intensively for transistors[11–13] except in very recent work.[14] Here, we report the fabrication and demonstration of chemically synthesized multilayer (s-) MoS_2 field-effect transistors (FETs) and compare the properties with exfoliated (x-) MoS_2 FETs.

s-MoS_2 flakes were grown by an iodine-transport method from previously synthesized MoS_2 (0.6 g) at 1060 K in an evacuated silica ampoule at a pressure of 10^{-3} Pa, and with temperature gradient of 6.8 K/cm. The volume concentration of iodine was 11 mg/cm^3. After 21 days of growth, the silica ampoule was slowly cooled to room temperature at a rate of 30 °C/h. The MoS_2 flakes were then dispersed by sonication in isopropyl alcohol (IPA) and transferred onto a 30 nm thick atomic-layer-deposited (ALD) Al_2O_3 dielectric on a $p+$ Si substrate held at 100 °C until dry. For comparison, x-MoS_2 flakes were released and transferred from bulk MoS_2 using scotch tape. The height of the MoS_2 flakes are in the range of 20–40 nm. Source and drain contacts were defined by electron beam lithography (EBL) using Ti/Au (5/100 nm) contacts. The devices were annealed at 300 °C for 3 h under Ar/H_2 flow to decrease the contact resistance. A schematic cross-sectional image of the back-gated (BG) MoS_2 device is shown in the inset of Fig. 1(a).

Figure 1(a) shows the measured drain current, I_D, per unit gate width, versus the back-gate-to-source voltage, V_{BG}, at room temperature for a multilayer s-MoS_2 channel at three drain biases. The gate modulation is $\sim 10^5$ and the gate leakage current is much lower (less than 1 pA/μm) than the drain current. This large gate modulation relative to graphene is attributed to the presence of a bandgap. The device shows clear n-type behavior indicating accumulation of electrons (n-type conductivity) for positive back-gate bias. The comparative transfer curves of x-MoS_2 FETs are also shown in Fig 1(a). s-MoS_2 and x-MoS_2 FETs show highly similar transfer characteristics. The extracted field-effect mobilities of both x-MoS_2 and s-MoS_2 FETs are ~ 30 cm^2/V s at room temperature. The subthreshold swing (SS) of the x-MoS_2 FET is 200 mV/dec. and that of the s-MoS_2 FET is 190 mV/dec. The average values of the FET mobility of each type of both x-MoS_2 and s-MoS_2 are ~ 15 cm^2/V s and the SS of those are ~ 170 mV/dec. Another s-MoS_2 (W/L $= 1/2\,\mu$m) FET is compared with x-MoS2 and electrical properties still work out to be similar.

The subthreshold swing is similar for the s-MoS_2 and x-MoS_2 FETs, but higher than the ideal Boltzmann limit of 60 mV/dec. The similar SS suggests that the interface charge leading to the higher subthreshold swing likely arises from

[a)]Electronic addresses: whwang@us.ibm.com and whwang1@nd.edu.
[b)]Electronic mail: djena@nd.edu.

 © 2013 American Institute of Physics

Downloaded 31 Jan 2013 to 129.74.250.206. Redistribution subject to AIP license or copyright; see http://apl.aip.org/about/rights_and_permissions

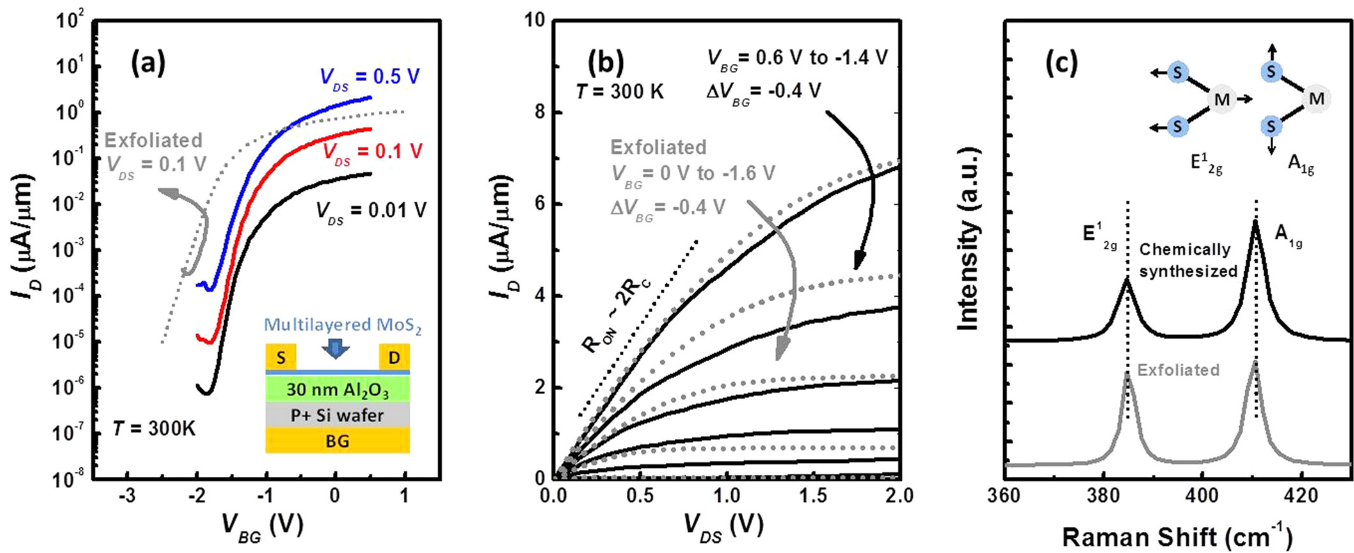

FIG. 1. Transport properties and Raman spectroscopy of FETs of s-MoS_2 with W/L = 1/2 μm and x-MoS_2 with W/L = 5/1.5 μm. (a) Drain current, I_D, per unit gate width vs. back-gate voltage, V_{BG}, of s-MoS_2 at various drain voltages, V_{DS}. The transfer curve of an x-MoS_2 is also shown for comparison, dotted line. (b) Common source transistor characteristics comparing s-MoS_2 (solid lines) and x-MoS_2 (dashed lines) FETs. (c) Raman spectra (λ_{exc} = 488 nm) of both s-MoS_2 and x-MoS_2 materials with a laser power of 1.5 mW and a spot size of 0.5-1 μm. The inset sketch shows the two primary vibrational modes in MoS_2 leading to the two peaks in the Raman spectrum.

traps in the Al_2O_3 dielectric, which are identical for the s-MoS_2 and x-MoS_2 FETs. The major difference between s-MoS_2 and x-MoS_2 FETs is in the threshold voltage. The flat-band voltage of the x-MoS_2 FETs is higher than that of s-MoS_2 by approximately 1 V. The possible reasons for this shift could be (a) different unintentional doping densities in s-MoS_2 and x-MoS_2, or (b) scotch tape residue-induced-charges possibly leading to a higher flat-band voltage for the x-MoS_2 compared to the s-MoS_2 FETs, which do not experience the tape exfoliation procedure. Identifying the precise reason for this threshold shift requires further work.

The family of I_D-V_{DS} curves at various V_{GS} in Fig. 1(b) shows typical transistor behavior including a linear increase of current at low V_{DS} and current saturation at high V_{DS}. The behavior shows desirable transistors attributes such as ohmic contacts, current saturation, and good gate electrostatic control. However, the current levels are in the μA/μm regime for micron long gate-lengths, which is low. The reason for the low current is a high contact resistance. The contact resistances of both s-MoS_2 and x-MoS_2 FETs in this work were extracted to be ~80 Ω mm at low V_{DS}. This value is comparable to the ~69 reported for exfoliated MoS_2 FETs.[6] This is an extremely high value, and currently holds back the performance of the FETs. The observation here is that s-MoS_2 and x-MoS_2 FETs have similar contact resistances, and are both high. A significant increase in the current drive of the FETs is expected if the contact resistance can be lowered to 1 Ω mm regime or lower, as is the case in Si and III–V FETs. The contact resistance can be lowered using a low work function metal like Sc.[15]

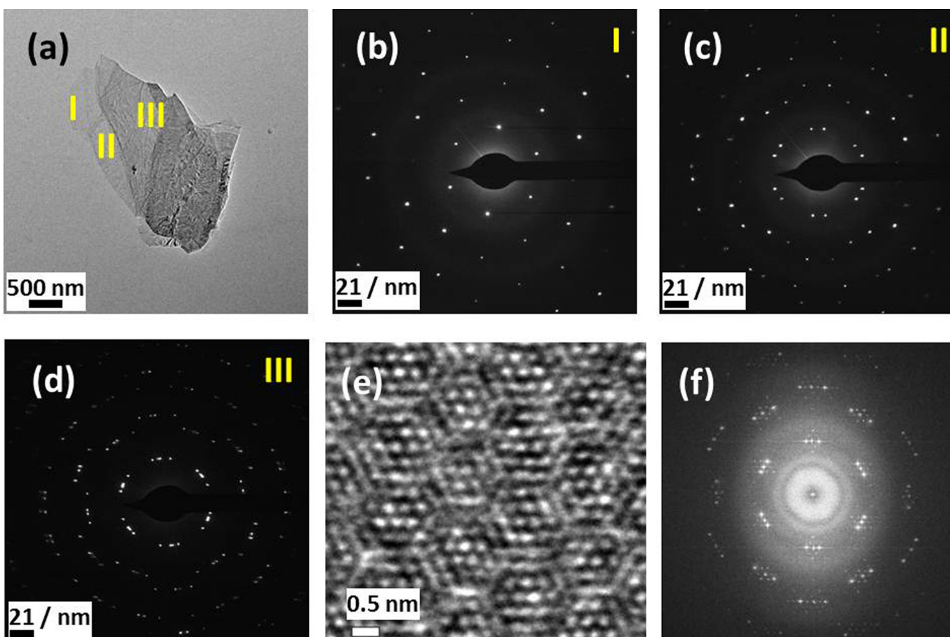

FIG. 2. (a) TEM of the s-MoS_2 multilayers. TEM electron diffraction patterns from (b) region I revealing the single crystal layer, (c) region II revealing the superposition of two single crystal layers with rotation, and (d) region III revealing the superposition of four single crystal layers with different rotations. The electron diffraction patterns reveal that the lattice parameter of s-MoS_2 is 0.32 nm. (e) An atomic-scale Moiré pattern of s-MoS_2 multilayers. (f) FFT from the image of (e), indicating three different crystal layers with different rotational angles.

Downloaded 31 Jan 2013 to 129.74.250.206. Redistribution subject to AIP license or copyright; see http://apl.aip.org/about/rights_and_permissions

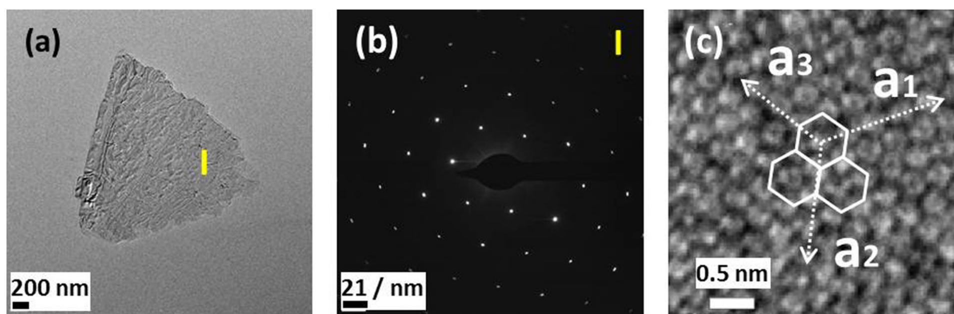

FIG. 3. (a) TEM of the x-MoS_2 multilayers. (b) Electron diffraction pattern from region I revealing the single crystal layer. (c) HR TEM image of region I. A lattice constant of 0.32 nm can be obtained from (b) and (c).

The measured Raman spectra shown in Fig. 1(c) at an excitation wavelength, λ_{exc}, of 488 nm are highly similar between s-MoS_2 and x-MoS_2 flakes. The spectrum exhibits two peaks: one in the $E_{2g}{}^1$ range, corresponding to in-plane vibrations at $\sim$385 cm^{-1}, and the other in the A_{1g} range corresponding to out-of-plane vibrations at $\sim$410 cm^{-1}. Since the Raman spectrum and transport properties are almost identical for s-MoS_2 and x-MoS_2, this confirms the overall similarity of chemically-synthesized and exfoliated MoS_2. In order to further investigate the atomic properties of s-MoS_2, transmission electron microscopy (TEM) was performed. The information obtained from s-MoS_2 is shown in Fig. 2 and compared with that of x-MoS_2 in Fig. 3.

Figure 2(a) shows the morphology of the s-MoS_2 on a TEM grid where a single crystal layer region (I), a superposition of two single crystal layer with rotation (II), and superposition of four single crystal layers with rotation (III) are clearly resolved. The corresponding TEM electron diffraction patterns are shown in Figs. 2(b)–2(d), respectively, showing the number of spots corresponding to the number of layers and the angular separation superimposed on the hexagonal lattice pattern. The electron diffraction patterns in Figs. 2(b)–2(d) reveal that s-MoS_2 flakes retain the crystal symmetry and lattice constant, $\sim$0.32 nm, when compared with that of x-MoS_2 in Fig. 3. A high-resolution (HR) TEM image is shown in Fig. 2(e) and its fast Fourier transform (FFT) is shown in Fig. 2(f). The FFT shows that the Moiré pattern in the image is due to three different crystal layers superimposed with different angles.

For comparison, the morphology of x-MoS_2 on the TEM grid and the electron diffraction pattern with a high-resolution TEM image are shown in Figs. 3(a)–3(c), respectively. The measurement confirms again a lattice parameter of x-MoS_2 of $\sim$0.32 nm which is identical to that of s-MoS_2 and that of bulk MoS_2.[16] The single-layer region is clearly resolved in the electron diffraction pattern, and the high-resolution atomic image clearly resolves the hexagonal crystal structure of single-layer MoS_2.

In summary, chemically synthesized MoS_2 transistors were fabricated and characterized, and compared with exfoliated MoS_2. The electronic and structural properties of chemically synthesized layers were found to be highly similar to exfoliated MoS_2. In particular, the transistor characteristics of s-MoS_2 were found to be almost identical to that of the x-MoS_2 in terms of FET mobility, subthreshold swing, on/off ratio, and contact resistance. TEM electron diffraction patterns and Raman measurements prove that the crystal symmetries and structural properties of s-MoS_2 are also identical to that of x-MoS_2. Though a number of issues need to be resolved before TMD crystals deliver high-performance transistors, this initial report shows that synthetic procedures can also realize high-quality channel material.

This work was supported in part by the Semiconductor Research Corporation (SRC), Nanoelectronics Research Initiative (NRI), and the National Institute of Standards and Technology (NIST) through the Midwest Institute for Nanoelectronics Discovery (MIND), the Office of Naval Research (ONR), and the National Science Foundation (NSF) Award No. 1232191 monitored by Dr. A. Kaul, and the Air Force Office of Scientific Research (AFOSR) Award No. FA9550-12-1-0257 monitored by Dr. J. Hwang. We thank J. Jelenc for technical help in crystal growth, Slovenian Research Agency of the Republic of Slovenia for financial support, Contract No. J1-2352 and the Centre of Excellence NAMASTE.

[1]K. S. Novoselov, A. K. Geim, S. V. Morozov, D. Jiang, Y. Zhang, S. V. Dubonos, I. V. Grigorieva, and A. A. Firsov, Science **306**, 666 (2004).
[2]Q. Zhang, T. Fang, H. Xing, A. Seabaugh, and D. Jena, IEEE Electron Device Lett. **29**, 1344 (2008).
[3]R. M. Feenstra, D. Jena, and G. Gu, J. Appl. Phys. **111**, 043711 (2012).
[4]L. Britnell, R. V. Gorbachev, R. Jalil, B. D. Belle, F. Schedin, A. Mishchenko, T. Georgiou, M. I. Katsnelson, L. Eaves, S. V. Morozov, N. M. R. Peres, J. Leist, A. K. Geim, K. S. Novoselov, and L. A. Ponomarenko, Science **335**, 947 (2012).
[5]B. Radisavljevic, A. Radenovic, J. Brivio, V. Giacometti, and A. Kis, Nat. Nanotechnol. **6**, 147 (2011).
[6]S. Kim, A. Konar, W. S. Hwang, J. H. Lee, J. Lee, J. Yang, C. Jung, H. Kim, J. B. Yoo, J. Y. Choi, Y. W. Jin, S. Y. Lee, D. Jena, W. Choi, and K. Kim, Nat. Commun. **3**, 1011 (2012).
[7]V. Podzorov, M. E. Gershenson, Ch. Kloc, R. Zeis, and E. Bucher, Appl. Phys. Lett. **84**, 3301 (2004).
[8]H. Fang, S. Chuang, T. C. Chang, K. Takei, T. Takahashi, and A. Javey, Nano Lett. **12**, 3788 (2012).
[9]D. Braga, I. G. Lezama, H. Berger, and A. F. Morpurgo, Nano Lett. **12**, 5218 (2012).
[10]W. S. Hwang, M. Remskar, R. Yan, V. Protasenko, K. Tahy, S. D. Chae, P. Zhao, A. Konar, H. Xing, A. Seabaugh, and D. Jena, Appl. Phys. Lett. **101**, 013107 (2012).
[11]Y. Shi, W. Zhou, A.-Y. Lu, W. Fang, Y.-H. Lee, A. L. Hsu, S. M. Kim, K. K. Kim, H. Y. Yang, L.-J. Li, J.-C. Idrobo, and J. Kong, Nano Lett. **12**, 2784 (2012).
[12]Y.-H. Lee, X.-Q. Zhang, W. Zhang, M.-T. Chang, C.-T. Lin, K.-D. Chang, Y.-C. Yu, J. T.-W. Wang, C.-S. Chang, L.-J. Li, and T.-W. Lin, Adv. Mater. **24**, 2320 (2012).
[13]Y. Zhan, Z. Liu, S. Najmaei, P. M. Ajayan, and J. Lou, Small **8**, 966 (2012).
[14]H. Wang, L. Yu, Y.-H. Lee, W. Fang, A. Hsu, P. Herring, M. Chin, M. Dubey, J. Kong, and T. Palacios, in *IEEE International Electron Devices Meeting* (2012), p. 4.6.1.
[15]S. Das, H.-Y. Chen, A. V. Penumatcha, and J. Appenzeller, Nano Lett. **13**, 100 (2013).
[16]P. A. Young, J. Phys. D: Appl. Phys. **1**, 936 (1968).

Downloaded 31 Jan 2013 to 129.74.250.206. Redistribution subject to AIP license or copyright; see http://apl.aip.org/about/rights_and_permissions